Gelation via Ion Exchange in Discotic Suspensions

Ya-Wen Chang, Andres F. Mejia, Zhengdong Cheng, Xiaojun Di, and Gregory B. McKenna

Phys. Rev. Lett. **108**, 247802 — Published 15 June 2012

DOI: 10.1103/PhysRevLett.108.247802

Gelation via Ion Exchange in Discotic Suspensions

Ya-Wen Chang[1], Andres Mejia[1], Zhengdong Cheng[1,2,3]*, Xiaojun Di[4], and Gregory B. McKenna[4]

[1] *Artie McFerrin Department of Chemical Engineering, Texas A&M University, College Station, Texas 77843, USA*

[2]*Material Science and Engineering Program, Texas A&M University, College Station, Texas 77843, USA*

[3]*Professional Program in Biotechnology, Texas A&M University, College Station, Texas 77843, USA*

[4]*Department of Chemical Engineering,Whitacre College of Engineering, Texas Tech University, Lubbock, Texas 79409, USA*

Received date

Abstract

Phase behavior of charged disk suspensions displays strong dependence on ionic strengths, as the interplay between excluded volume and electrostatic interactions determines the formation of glasses, gels, and liquid crystal states. The various ions in natural soil or brine, however, could present additional effects, especially considering most platelet structures bear momentous ion-exchange capacity. Here we observed how ion exchange modulates and controls the interaction between individual disks and leads to unconventional phase transitions from isotropic gel to nematic gel, and finally to nematic liquid crystals.

PACS numbers: 64.70.mj, 83.80.Hj, 82.70.Dd, 82.70.Gg

Colloidal dispersions of charged anisotropic particles exhibit an intriguingly wide range of rheological properties and rich liquid crystal phase behaviors. The ability of non-spherical particles to undergo spontaneous disorder-to-order, i.e., isotropic-to-nematic (I-N), liquid crystal transition at high particle concentrations was first demonstrated theoretically by Onsager [1] as a purely entropy-driven process due to particle-shape anisotropy. Stable liquid crystal phases formed by plate-like particles were later confirmed by computer simulations [2-3]. In addition, disordered states, such as gels or glasses, are particularly prominent in charged systems [4-6]. They were thought always to intervene with the observation of stable nematic phases, with the most notable example of non-reproducible I-N separation in hectorite suspensions observed by Langmuir [7]. However, research in the past decade has revealed the existence of nematic phases for selected natural and synthetic clays [8-10], whose I-N transition occurred at concentration lower than the sol-gel transition point that is strongly dependent on the ionic strength of the solvent. To date, there seems to be little work showing the ionic strength controlled phase diagrams of charged, discotic suspensions that display both gel phase and stable liquid crystal phases. The detailed study here will elucidate gelation of discotic suspensions that readily form liquid crystal phases under normal conditions. These gels are vastly different from structures of nematic liquid crystal embedded in a secondary matrix, the so-called nematic gels [11-12]. The ability to precisely describe gel structure and its formation in such systems is of vital importance to their technological applications such as use as rheology modifiers and fillers in composite materials.

Aqueous suspension of high-aspect-ratio, charge-stabilized zirconium phosphate (ZrP) platelets prepared by exfoliation was recently shown to exhibit stable nematic alignment at low-

volume fractions [13]. As with clay, the ion-exchange property of α-ZrP has long been exploited in applications such as nuclear waste treatments and kidney dialysis; hence, its structure and physiochemical properties are well characterized. In this letter, we present the phase diagram of these equal-thickness platelets as a function of salt and particle concentrations. Different phases were distinguished and characterized with polarized imaging, rheology, and light scattering. We find that a strong specific attraction induced by ion exchange leads to gelation of the suspension; conversely, with insufficient ion exchange, repulsive interactions remain dominant, drawing the system back to liquid crystal state.

We synthesized α-zirconium phosphate pristine (layered) crystals using a hydrothermal procedure[14], and exfoliated them with tetrabutyl ammonium hydroxide (TBAOH) at a molar ratio of TBAOH: α-ZrP=1:1 to obtain stable colloidal suspensions of monolayered ZrP in deionized water. Excess TBAOH was removed by centrifugation at 4000 g for 2 hours, and the platelets were resuspended in deionized water. Completely exfoliated platelets have an identical thickness of 2.68 nm [15-16] and an average diameter D, determined by dynamic light scattering. Several batches (B1~B4) of particles were prepared in this study, and minimal variations in size and polydispersity were present (D= 1325 nm, polydispersity σ = 32% for B1 batch; D = 1093 nm, σ = 32% for B2 batch; D = 1485 nm, σ = 36% for B3 batch; D = 1431 nm, σ = 34% for B4 batch). Concentration of the stock suspension was determined gravimetrically by drying a fixed amount of the suspension at 60°C. Stock suspensions were diluted with deionized water or salt solutions to obtain the desired particle concentrations and ionic strengths.

We investigated the influence of ionic strength on the I-N transition of ZrP suspensions. Tetrabutylammonium chloride (TBACl), a salt with an identical cation to the exfoliating agent, was chosen first to avoid complication of the system, and the samples were monitored through

cross-polarizers. Fig. 1a shows cross-polarized photographs of monolayer platelets at ten concentrations, increasing from left to right, suspended in 0- to 100- millimolar ionic strength solutions. For a fixed ionic strength, very dilute particle suspensions showed strong flow birefringence under cross-polarizers. At increased particle concentrations (in the I-N coexistence region), the suspensions became permanently birefringent and exhibited nematic defects in polarizing microscopy (Fig 1b). Over the course of 48 hours, complete phase separation occurred for these two-phase coexistent samples into an upper isotropic and lower nematic phase, separated by a visibly sharp interface. Fig. 1c gives a snapshot of the progressive increase of nematic volume fraction in the samples with the overall platelet weight fraction for varying ionic strengths. At fixed particle concentrations (weight fraction ϕ_w) within the biphase region, the nematic appears increasingly compressed with the increase of ionic strengths, a phenomenon anticipated as a result of the decrease in repulsion as is observed in clays [17]. The boundaries of the biphasic gap can be extrapolated by a nonlinear fit (due to wide polydispersity [13]) in Fig. 1c to the height-concentration curve. Fig. 1d summarizes the TBACl-dependent phase diagram: The lower boundary $\phi_{w,I}$ was essentially unchanged up to ionic strength of 10 mM; Full nematic phase $\phi_{w,N}$ was obtained at $0.011 \leq \phi_{w,N} \leq 0.014$ for ionic strengths below 1 mM, $\phi_{w,N} \sim 0.017$ for 10 mM, and $\phi_{w,N} > 0.022$ for 100 mM (exact position not determined). This increase in $\phi_{w,N}$ with ionic strength is in qualitative agreement with the screening of electrostatic repulsion with ions. In the study of crystallization in suspensions of charged colloidal spheres, fluid-crystal coexistence increases with ionic strength to a maximum at the hard sphere limit [18].

Theoretical calculations on infinitely thin hard platelets [2] have shown that I-N phase transitions occur between densities $\rho_{iso} D^3 = 3.7$ and $\rho_{nem} D^3 = 4.0$ for monodispersed suspensions, where ρ is number densitiy of the transitions and D, the platelet diameter. Since our

system exhibits high polydispersity, it is reasonable to compare experimental with the theoretical values for polydispersed samples ($\sigma \sim 32\%$), whose densities are found to be $\rho_{iso}D^3 = 3.5$ and $\rho_{nem}D^3 = 5.6$ (according to ref [2]). Following van der Beek and Lekkerkerker [9], the relation between core volume fraction ϕ and number density for platelets of diameter D, thickness t, and polydispersity σ is

$$\rho\langle D\rangle^3 = 8/9\sqrt{3}\left(\langle D\rangle/\langle t\rangle\right)\left(1+3\sigma^2\right)/\left(1+\sigma^2\right)\phi. \quad (1)$$

Taking into account the geometrical factor after exfoliation (layer thickness increased by three-fold due to the attachment of TBA^+), we convert weight percents into disk ϕ values by an approximate density value of ~1.8 g/cm^3. Eq. (1) yields dimensionless densities of $\rho_{iso}D^3 = 2.1$ and $\rho_{nem}D^3 = 5.2$ for our suspensions at zero ionic strength. The results are comparable to theoretical values; discrepancies might be due to platelet geometry or surface charges.

In addition to liquid crystal phases, gelled phases occurred when a common salt—sodium chloride (NaCl)—was used to adjust suspension ionic strength instead of TBACl. Fig. 2 presents the optical photographs of series of suspensions in 0 (as reference for salt-free phase diagram), 10, and 20 mM NaCl, providing preliminary evidence of gelled states, in which samples were able to retain air bubbles due to finite yield stresses. Gelled samples at platelet concentration below $\phi_w = 0.011$ for both 10 mM and 20 mM ionic strength appeared isotropic; for 20 mM series, those whose concentrations were between $0.011 \leq \phi_w \leq 0.021$, on the other hand, displayed strong birefringent textures. For 10 mM ionic strength series, re-entrance of stable liquid crystalline phase was found at concentrations above 0.011. Biphasic samples (with clear phase separation) were observed at $0.011 \leq \phi_w \leq 0.021$, within which the proportion of lower nematic phase increases with the concentration of particles. Full nematic fluid was obstained at $\phi_w \approx 0.028$. Similarly, for 20mM series, the suspensions appeared fluid again at $\phi_w > 0.021$ (Fig.

S2). The nature of these higher particle and salt concentration samples is less obvious as they appear diffusive in bulk (path length ~9mm) due to the high refractive index of zirconium phosphate. As flocculated samples could also appear birefringent in consequence of scattering from aggregated (anisotropic) clusters, it is important to demonstrate sample homogeneity via bright-field imaging. The absence of optical contrast viewed in regular light (Fig. S3) verifies its homogenous nature, and the suspension can be recognized as liquid crystalline phase by the pronounced optical texture under polarized microscopy imaging, similar to that in zero ionic strength (Fig. 2 right).

Formation of gel structures were further verified and characterized with rheology and light-scattering measurements. Small-amplitude oscillatory shear experiments were carried out using a Parr-Physica MCR-300 rheometer with parallel plate geometry (25-mm plate diameter, gap of 0.5mm) at 25°C. The samples were pre-sheared at 500 s^{-1} and relaxed for 8 min. The elastic and viscous moduli G′ and G″ were measured at a strain amplitude of $\gamma = 0.02$ with angular frequencies from 0.01 s^{-1} to 100 s^{-1} (Fig. S2). Fig. 3a shows the elastic modulus G′ (value at 1 s^{-1}) as a function of ϕ_w at 20mM NaCl for selected gel samples from B3 batch, where the reduced positive dependency of G′ with particle concentrations is demonstrated. The result differs dramatically from previous studies on anisotropic colloidal gels [19-21], whose storage modulus followed a power law dependence on reduced particle volume fraction $(\phi-\phi_0)^n$ at fixed ionic strength (n = 2.3~2.5 for clay suspensions, ϕ_0 is the critical ϕ above which gel appears). At this salt concentration, the gel characteristic eventually disappeared at $\phi_w > 0.021$.

Multi-speckle diffusive wave spectroscopy (DWS) in backscattering geometry [22-23] was used to identify arrested/non-arrested structures. The samples were illuminated with a 633-nm

laser, and the backscattered light was collected onto a CCD camera at 90 frames/s. The ensemble average autocorrelation function is obtained from

$$g_2(t) = \langle I_i(0) I_i(t) \rangle / \{ \langle I_i(0) \rangle \langle I_i(t) \rangle \} \quad (2)$$

where I_i refers to the intensity of backscattering light at the i^{th} pixel, which is a function of time. The correlation function g_2 quantitatively describes the similarity between two images at different times. In general, relaxation time (or decorrelation time) is defined as the time required for g_2 to decay to half its value at time zero. Slower decay of g_2 or longer relaxation time indicates slower particle motions, a sign for restricted motion for frozen systems such as glassy materials and colloidal gels. Fig. 3b shows g_2 versus time for six samples (B4 batch) at aging time around 2 hours, with concentrations span through broader phase states than that included in Fig. 2a— isotropic gel (sample 1 and 2), nematic gel (sample 3 and 4) , and fluidic liquid crystal phase (sample 5 and 6). Correlation functions of samples 1~4 showed significant long relaxation time, typical of arrested states. Dramatic relaxation-time reduction was apparent for higher concentration samples (5 and 6), confirming un-gelling transition when ϕ_w increased from 0.021 to 0.028 (B4 batch, 20mM NaCl). Additionally, aging phenomenon (the evolution of the correlation function with time) was observed for gel-state samples while being absent for liquid crystal samples (data not shown), providing corroborating evidence for the transition.

The liquid crystal and sol-gel phase behaviors in NaCl solutions were evaluated using the above-described methodologies (see supplementary information) and mapped onto a two-dimensional phase diagram (Fig. 4). At salt concentrations below 10mM, the offset of phase boundaries is qualitatively consistent with the TBACl case. In contrast to the TBACl system, where the dispersion appears stable up to 100mM ionic strength, gelation occurred for NaCl concentrations larger than 10mM. The location of the gel region determined by rheology and

light-scattering data infers unprecedented gel-to-liquid crystal transitions upon increasing particle concentration at fixed ionic strengths. Although arrested states are encountered frequently in charged platelet systems, the phase behavior of the NaCl-ZrP system is different from the gelling behavior observed for most natural or synthetic clays, where the percolated networks expand throughout the entire sample with particle concentrations above the sol-gel transition [8, 17, 20-21, 24]. The unique phase evolution pathway suggests an intrinsically different mechanism for the gelling behavior of ZrP platelets in the presence of NaCl.

To rationalize this unusual phase behavior, we take a closer look at the structure of the monolayer platelets, the origin of the gel phase, and how the surface charges and inter-particle interactions are modified with the addition of NaCl. Since the exfoliated monolayer platelet $Zr(HPO_4)(TBAPO_4)$ consists of half-exchanged α-ZrP, with a layer of TBA^+ packing on the platelet surface and an underlying residual hydroxyl group in between each TBA^+, ion exchange could proceed in the presence of NaCl as Na^+ displaces the available protons or the loosely bound TBA^+ on the surfaces (Fig. S5). Release of the dissociated H^+ is into the suspension from the proton displacement process can be detected, as shown in Fig. 5 a significant, continuous drop of suspension pH with the addition of NaCl until a plateau value of ~3.3 was reached. The suspension enters arrested state at approximate equal molar ratio of NaCl to ZrP, where the pH value drops below 5.5. Direct acidification using HCl also yield similar sol-gel transition (data not shown), indicating that pH = 5.5 is the critical point where strong attraction arises, presumably in the face-edge direction due to opposite charges at the rims and faces of the platelets (supplementary).

From the aspect of ion exchange, interpretation of the phase behavior as a function of NaCl concentration and packing fraction can now be refined as follows. At low ionic strength (0 to 7.5

mM), where the effect of surface charge alteration is minimal due to limited ion exchange (molar ratio of $Zr(HPO_4)(TBAPO_4)/NaCl >>1$), the influence of ionic strength can be considered to be an electrostatic screening one, similar to TBACl cases. At higher ionic strengths and low particle concentrations (NaCl >7.5mM, $Zr(HPO_4)(TBAPO_4)/NaCl \leq 1$), ion exchange between Na^+ ions and surface protons reduces the suspension pH below 5.5, a transition from repulsive to attractive interactions takes place, causing gelled phases to appear. The decrement in suspension pH (i.e., concentration of protons released), controlled by the degree of ion exchange, is roughly proportional to NaCl concentration and inversely proportional to particle concentration according to the chemical balance of the exchange reaction. Therefore, for constant ionic strength, the degree of ion exchange decreases with increasing particle volume fraction (less pH reduction), which leads to an overall weaker attraction at higher particle concentrations. This explains the gel-to-liquid crystal transition upon increasing platelet fractions that's consistent with the generally trend of jamming phase transitions (as change in interaction potentials) [25].

In summary, we have studied the ionic strength dependent phase diagram of ZrP monolayer platelets, and validated the use of ion exchange to induce anisotropic interactions among individual platlelets. Liquid crystal states and arrested states were identified and confirmed via polarized imaging, rheology and diffusive wave scattering techniques. Unlike regular clay suspension cases, fluidization occurs at increasing particle concentrations for (NaCl) ionic strength above ≈ 8 mM, where low-volume fraction gels started to form. The gelling transitions were shown to depend strongly on suspension pH (consequence of ion exchange at different NaCl/ZrP ratios), a parameter expected to influence charge interactions. The results offer a novel observation of the gelling behavior of charged discotic suspensions as ion exchange (pH) - modulated interactions come into play. Our work opens up new routes to the formation of

discotic colloidal gels, and the comparison with other charged platelet systems should contribute to a better understanding of the role of ion exchange that is fundamental to charged discotic materials.

Acknowledgement

We thank Y. Martinez-Raton, E. Velasco, and A. Clearfield for discussions useful to the content of this paper. Acknowledgment is made to V. Ugaz for the use of the MCR rheometer. This work is supported by NSF DMR-1006870 at TAMU and NSF CBET-1133279 at Texas Tech University.

Figure captions

FIG. 1 (color online). Influence of TBA salt concentration on ZrP platelet phase diagram. (a) Polarized light photograph of ZrP platelet suspensions at particle concentrations of 0.28, 0.56, 0.69, 0.83, 1.11, 1.39, 1.67, 1.94, 2.22, 2.50 wt% in TBACl solutions. (b) Schlieren texture of a nematic suspension. Scale bar: 150μm. (c) Nematic height as a function of salt and particle concentrations. (d) Summarized phase diagram. Phase states include isotropic liquid (open rectangle), biphasic (half-filled rectangle), and nematic (filled rectangle). Dashed curve outlines the biphase region.

FIG. 2 (color online). Polarized images of ZrP suspensions (B3 batch) in 0, 10, and 20 mM NaCl salt solutions. Left: Photograph of bulk samples at increasing ϕ(left to right, labeled concentration in wt%). Right: Micoscopy images of high concentration liquid crystal phases. Scale bar: 50μm

FIG. 3 (color online). (a) Evolution of the elastic modulus as a function of platelets (B3 batch) concentration at an ionic strength of 20mM. (b) Autocorrelation functions of varying ZrP (B4 batch) concentrations (from 1 to 6, 0.36, 0.71, 1.07, 2.13, 2.84, 4.26 %) at fixed NaCl concentration and aging time (~2hr).

FIG. 4 (color online). State diagram as a function of platelet and NaCl concentration. Phase states include isotropic liquid (open rectangle), isotropic gels (open circle), birefringent gels (half-filled circle), biphasic (half-filled rectangle), and nematic (filled rectangle) liquid crystals. Shaded areas represent the gelled phase, and the biphase region is outlined for both polydispersed (B3 batch, dashed lines) and more monodispersed (B2 batch, crosses linked with solid lines) samples.

FIG. 5 (color online). Suspension pH evolution with added NaCl concentration. Insert: pH at broader NaCl/ZrP ratios.

Figures

Fig. 1

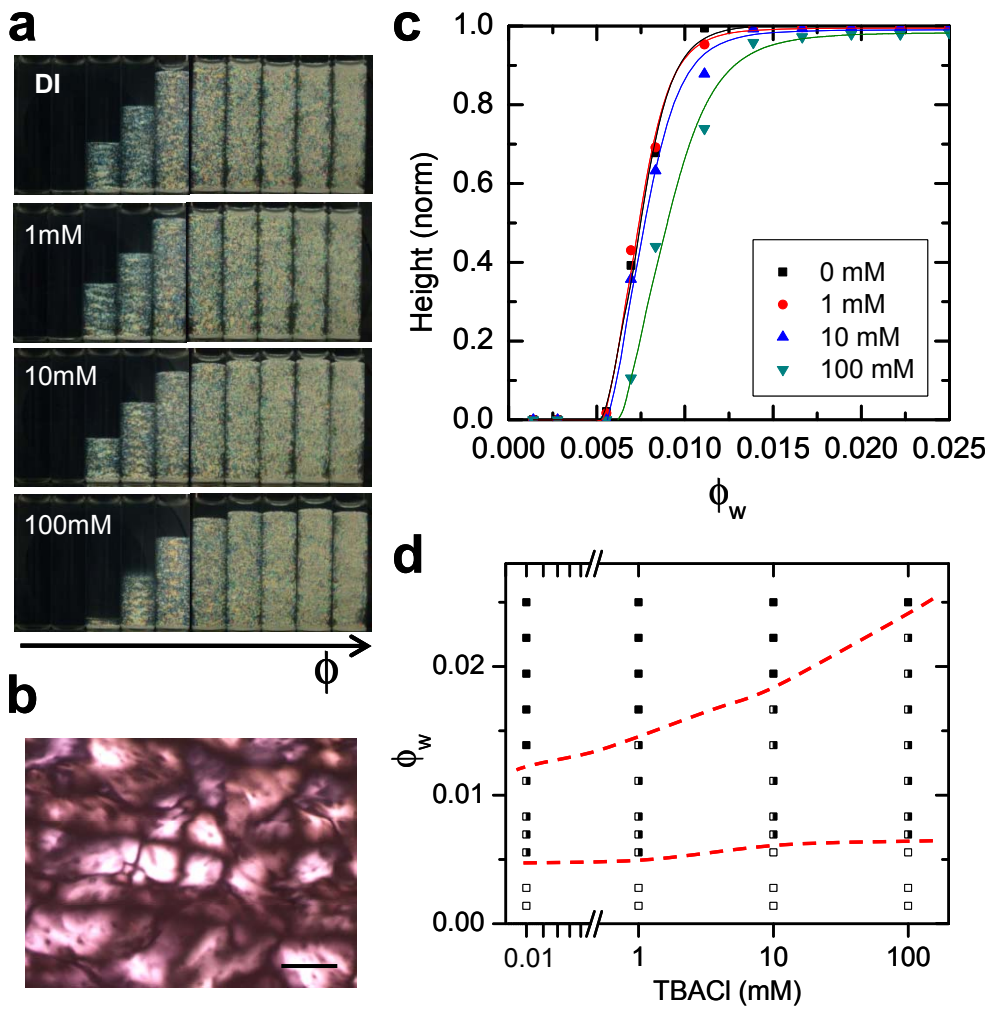
a
DI
1mM
10mM
100mM
ϕ
b
c
1.0
0.8
0.6
0.4
0.2
0.0
Height (norm)
0.000 0.005 0.010 0.015 0.020 0.025
ϕw
0 mM
1 mM
10 mM
100 mM
d
0.02
0.01
0.00
ϕw
0.01
1
10
100
TBACl (mM)

Fig. 2

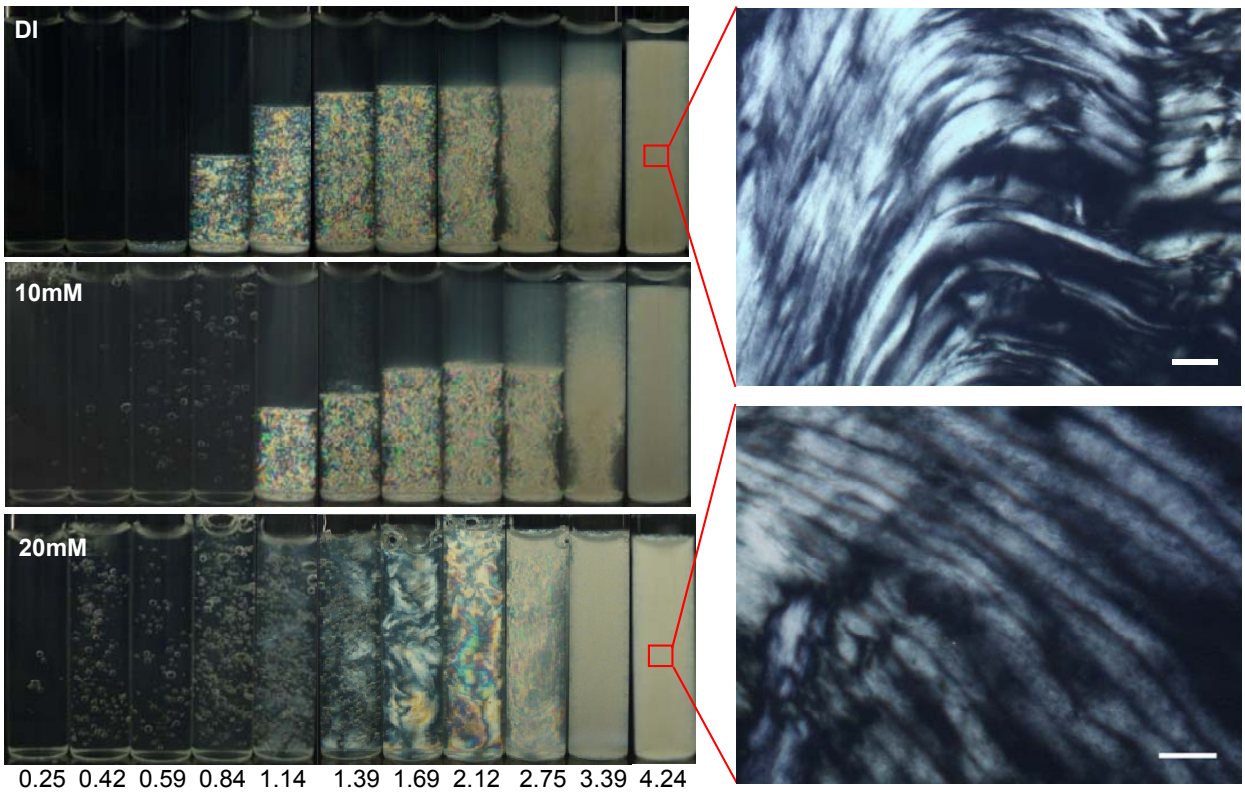
DI
10mM
20mM
0.25 0.42 0.59 0.84 1.14 1.39 1.69 2.12 2.75 3.39 4.24

Fig. 3

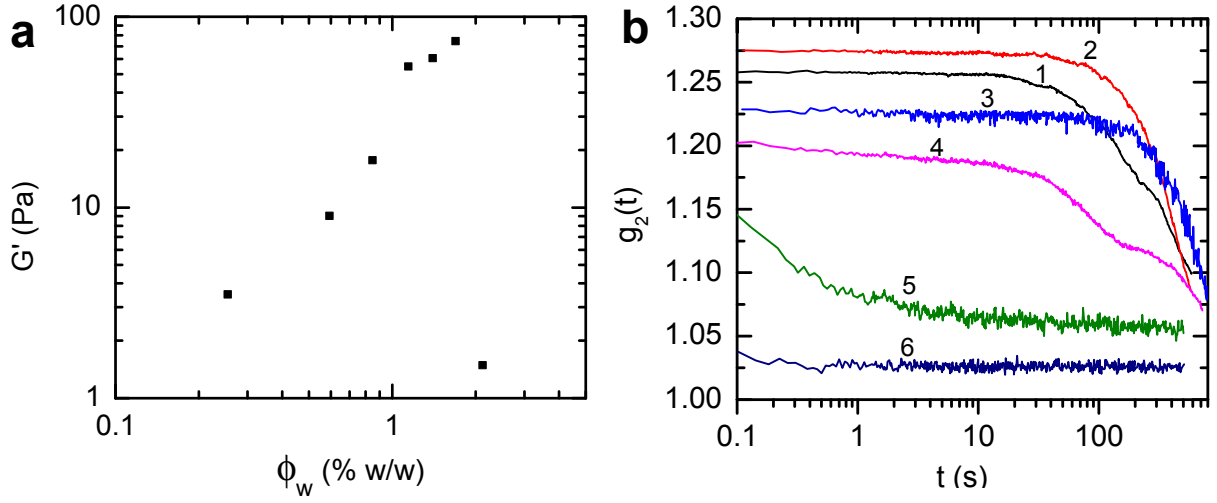
a
100
10
1
G' (Pa)
0.1
1
ϕ_w (% w/w)
b
1.30
1.25
1.20
1.15
1.10
1.05
1.00
$g_2(t)$
1
2
3
4
5
6
0.1
1
10
100
t (s)

Fig.4

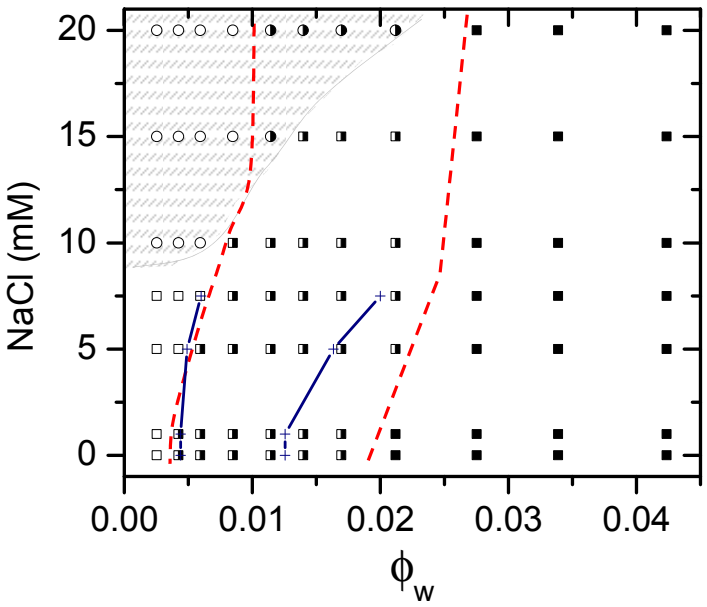
NaCl (mM)
20
15
10
5
0
0.00
0.01
0.02
0.03
0.04
ϕ_w

Fig.5

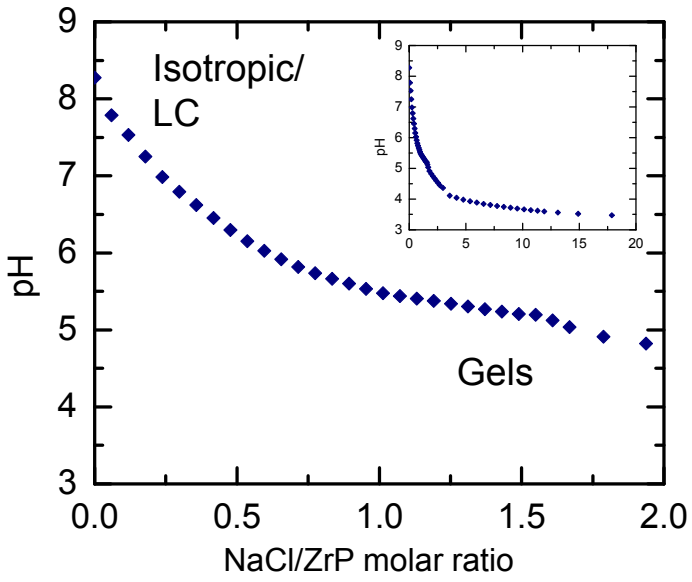
pH
9
8
7
6
5
4
3
0.0
0.5
1.0
1.5
2.0
NaCl/ZrP molar ratio
Isotropic/
LC
Gels
pH
9
8
7
6
5
4
3
0
5
10
15
20

References

[1] L. Onsager, Annals of the New York Academy of Sciences **51**, 627 (1949).
[2] M. A. Bates, and D. Frenkel, Journal of Chemical Physics **110**, 6553 (1999).
[3] J. A. C. Veerman, and D. Frenkel, Physical Review A **45**, 5632 (1992).
[4] D. van der Beek, and H. N. W. Lekkerkerker, Europhysics Letters **61**, 702 (2003).
[5] J. C. P. Gabriel, C. Sanchez, and P. Davidson, Journal of Physical Chemistry **100**, 11139 (1996).
[6] A. Mourchid *et al.*, Langmuir **11**, 1942 (1995).
[7] I. Langmuir, Journal of Chemical Physics **6**, 873 (1938).
[8] L. J. Michot *et al.*, Proc. Natl. Acad. Sci. U. S. A. **103**, 16101 (2006).
[9] D. van der Beek, and H. N. W. Lekkerkerker, Langmuir **20**, 8582 (2004).
[10] H. Hemmen *et al.*, Langmuir **25**, 12507 (2009).
[11] T. C. Lubensky *et al.*, Physical Review E **66**, 011702 (2002).
[12] D. Lacoste, A. W. C. Lau, and T. C. Lubensky, European Physical Journal E **8**, 403 (2002).
[13] D. Z. Sun *et al.*, Physical Review E **80**, 041704 (2009).
[14] L. Y. Sun *et al.*, New Journal of Chemistry **31**, 39 (2007).
[15] H.-N. Kim *et al.*, Chemistry of Materials **9**, 1414 (1997).
[16] L. Sun *et al.*, Chemistry of Materials **19**, 1749 (2007).
[17] N. I. Ringdal *et al.*, Physical Review E **81**, 041702 (2010).
[18] W. B. Russel, D. A. Saville, and W. R. Schowalter, in *Colloidal Dispersions* (Cambridge University Press, New York, NY, 1999), p. 347.
[19] L. J. Michot *et al.*, Langmuir **25**, 127 (2009).
[20] A. Mourchid *et al.*, Langmuir **14**, 4718 (1998).
[21] L. J. Michot *et al.*, Langmuir **20**, 10829 (2004).
[22] V. Viasnoff, F. o. Lequeux, and D. J. Pine, Review of Scientific Instruments **73**, 2336 (2002).
[23] X. J. Di *et al.*, Phys. Rev. Lett. **106** (2011).
[24] M. C. D. Mourad *et al.*, J. Phys. Chem. B **113**, 11604 (2009).
[25] V. Trappe *et al.*, Nature **411**, 772 (2001).